Microaneurysms Detection with the Radon Cliff Operator in Retinal Fundus Images.

Luca Giancardo[a,b], Fabrice Meriaudeau[b], Thomas P. Karnowski[a], Kenneth W. Tobin[a], Yaqin Li[c] and Edward Chaum, M.D.[c]

[a]Oak Ridge National Laboratory, Oak Ridge TN, USA;
[b]University of Burgundy, France;
[c]Hamilton Eye Institute, U. Tennessee Health Sciences Center, Memphis TN, USA

ABSTRACT

Diabetic Retinopathy (DR) is one of the leading causes of blindness in the industrialized world. Early detection is the key in providing effective treatment. However, the current number of trained eye care specialists is inadequate to screen the increasing number of diabetic patients. In recent years, automated and semi-automated systems to detect DR with color fundus images have been developed with encouraging, but not fully satisfactory results. In this study we present the initial results of a new technique for the detection and localization of microaneurysms, an early sign of DR. The algorithm is based on three steps: candidates selection, the actual microaneurysms detection and a final probability evaluation. We introduce the new *Radon Cliff* operator which is our main contribution to the field. Making use of the Radon transform, the operator is able to detect single noisy Gaussian-like circular structures regardless of their size or strength. The advantages over existing microaneurysms detectors are manifold: the size of the lesions can be unknown, it automatically distinguishes lesions from the vasculature and it provides a fair approach to microaneurysm localization even without post-processing the candidates with machine learning techniques, facilitating the training phase. The algorithm is evaluated on a publicly available dataset from the Retinopathy Online Challenge.

Keywords: radon transform, diabetic retinopathy, segmentation

1. INTRODUCTION

Diabetic retinopathy is a progressive disease, and a timely intervention is the best way to avoid the risk of vision loss and blindness in patients. Color fundus images have been proven to be an effective and relatively inexpensive way to diagnose diabetic retinopathy. Human readers are able to screen patients by visually inspecting the images of the fundus looking for lesions typical of the condition. However, the shortage of trained readers makes widespread screening of diabetic patients difficult, and for this reason various techniques have been proposed to partially or fully automate the screening process.

The lesions typical of non-proliferative diabetic retinopathy include hemorrhages, exudates and microaneurysms among others. In this work we will present a new technique to automatically segment microaneurysms. This type of lesion occurs early and may be most useful for screening purposes; it consists of a swollen capillary that appears as a small red spot in the fundus. From an image processing standpoint the automatic detection of the microaneurysms present various challenges:

- Their color and size is the same as the vessels (in fact they are small vessels themselves).
- They have a variable size and often they are so small that can be easily confused with the images noise (or vice versa).
- Even expert ophthalmologists do not always agree whether a red lesion is a microaneurysm or small dot hemorrhage. The only way to be certain is through fluorescein angiography, an invasive procedure which involves the injection of a contrast agent in the patient.
- The human retina has a large degree of variability; pigmentation, texture and size and position of human features change from person to person.

Medical Imaging 2010: Image Processing, edited by Benoit M. Dawant, David R. Haynor,
Proc. of SPIE Vol. 7623, 76230U · © 2010 SPIE · CCC code: 1605-7422/10/$18 · doi: 10.1117/12.844442

Downloaded from SPIE Digital Library on 03 May 2010 to 128.219.49.8. Terms of Use: http://spiedl.org/terms

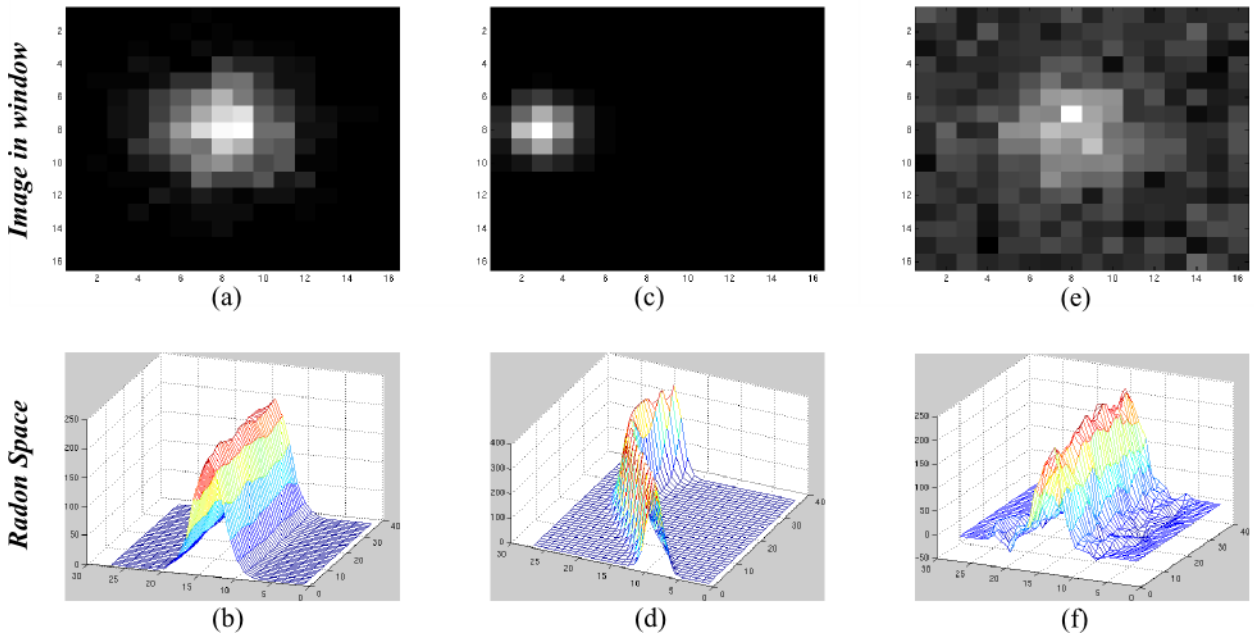

Figure 1. Appearance in the Radon space of difference Gaussian structures.

We will present a novel operator (the Radon Cliff) based on the Radon Transform, which is exhibits a strong response to microaneurysms because of their round Gaussian-like structures. The Radon Transform is well known in the Medical Imaging field as a technique to reconstruct a two or three dimensional object from its projections.[1] While its usage for other purposes is uncommon, it is possible to find its application in image compression[2] and in texture characterization.[3] The Radon Cliff Operator works in the Radon space exploiting the compact representation of the data provided in order to detect Gaussian-like structures of variable size in a sliding window, even when noise or vessels are present.

In section 2 we introduce the details of the Radon Cliff operator and an example of how it can be employed in the segmentation process; then the preliminary results are presented in section 3. Finally, section 4 and 5 will analyze the results and conclude the discussion.

2. METHOD

The algorithm proposed for the detection of microaneurysms is composed of three phases. First, the image is normalized and the candidate lesions are extracted. Second, the Radon Cliff operator is used to extract specific measurements from the candidates. Finally, in a post-processing phase, the various measures are evaluated and a final posterior probability is generated for each lesion candidate.

We will start with a description of the *Radon Cliff* operator, illustrating the appearance of Gaussian-like shapes in the Radon space and how two descriptive features can be extracted; then, the ways employed to pre-process the image and a complete description of the current technique employed to detect microaneurysms will be presented.

2.1 Radon Cliff Operator

The operator lays its foundations on one observation: every roughly circular Gaussian shape appears as a continuous chain of cliffs if observed in the Radon space. The morphology of the cliffs describes three properties of the circular Gaussian shape: its relative location in the window, its size and intensity. The location in the window can be deduced from the shape of the crest, which is a straight line if the Gaussian is located at the center of the window or another type of curve if the Gaussian is otherwise situated in the window (see Fig 1.(b,d)). The size and intensity are given respectively by the width and height of the cliffs. Fig 1.(e,f) shows how this cliff-like structure is insensitive to a conspicuous amount of noise.

Downloaded from SPIE Digital Library on 03 May 2010 to 128.219.49.8. Terms of Use: http://spiedl.org/terms

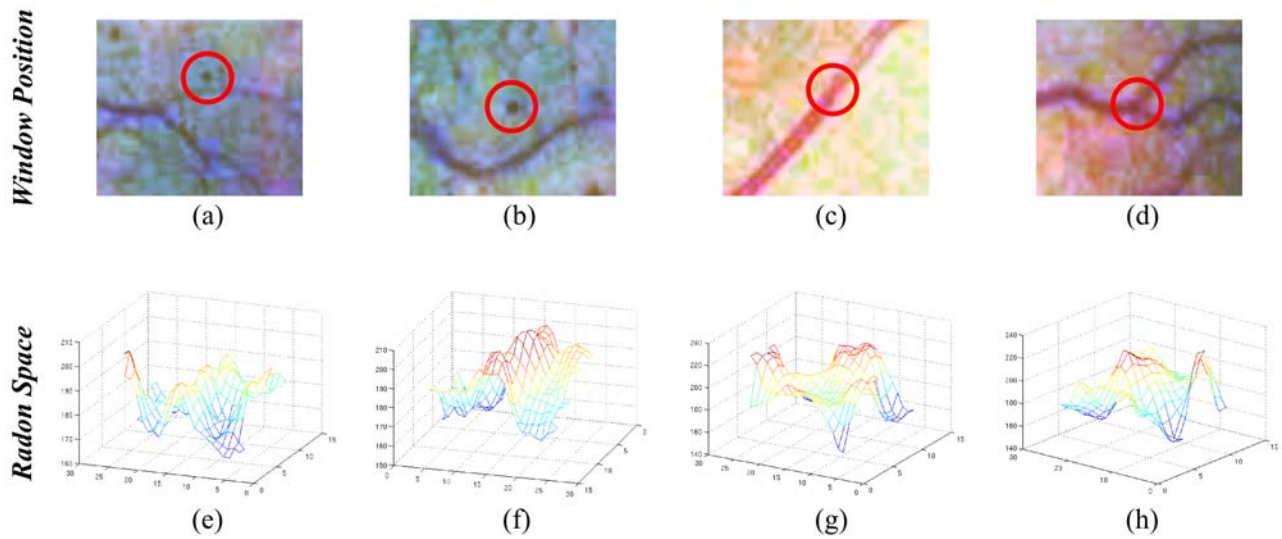

Figure 2. Appearance in the Radon space of microaneurysms attached to vessels (a,e) (b,f) and vessels themselves (c,g) (d,h). Note that the red circle in the first row represents the area of the window for the Radon transform.

There are other advantages to analysis in the Radon space. When detecting the targeted structure in a window with other techniques based on template matching, the target must be the most prominent object in the window. Hence, an algorithm based on this type of technique needs to go through a training phase to find a window containing the target with enough space to contain the support background, but sufficiently small to avoid any external object. Similar problems occur when a template function is dynamically adapted to the window using least mean square or other regression approaches. On the other hand, the analysis in the Radon space greatly simplifies the identification of a Gaussian-like object in a window containing another structure with a higher pixel values. If the Gaussian object is at the center of the window, it will maintain the continuous cliff-like appearance, and the other object will appear as a protrusion which might be connected or disconnected to the central structure. In the context of microaneurysms detection this aspect is of a particular importance since many lesions of this type tend to appear close to big vessels or capillaries (see Fig 2.(a,b)).

For our purposes, the Radon transform must be applied in a small window with a low sampling rate [*]. Therefore, the Radon projections at some angles will go through an unequal number of pixels, which leads to an image containing coefficients biased towards certain locations. The problem is accentuated even more by the square shape of the pixels: some neighbouring rays of the Radon projections tend to go through the same pixel more than once and others do not. This problem is particularly apparent when the Gaussian target lays over a background with a high pixel value mean. We overcome this "Radon transform bias" by normalising each projection in each angle for the number of pixels the projection ray goes through; effectively making each coefficient in the Radon space the mean value of the pixels crossed by each projection rays for each angle. The normalization can be obtained efficiently by initially applying the Radon transform on a image containing only ones and having the same size of the sliding window, then using it to divide the coefficient obtained by applying the Radon transform on the sliding window.

In all the examples of Fig 1 and Fig 2 the key invariant characteristic is the continuity of the crests in all the Radon projections that form the space. This holds even if other objects visible in the window, the only difference is that the central cliff-like structure will have a relative shorter height. In principle, it is possible to detect the Gaussian-like structure regardless of its position in the window; however from a practical standpoint constraining the detection to the center of the window facilitates the design of the operator. Also, Fig 2.(g,h) show how the continuity of the crest disappears on vessels and vessel junctions. The *Radon Cliff operator* proposed will output two measures: the *path votes* (*pVotes*) and *cumulative peak probability* (*CPP*).

The *path votes* provide a measure of the continuity of the path that corresponds to the blob at the center of the window. If the blob resembles a Gaussian it will receive positive votes, otherwise negative ones. The first step is the calculation of

[*] the sampling rate in this context corresponds to the number of pixels.

Downloaded from SPIE Digital Library on 03 May 2010 to 128.219.49.8. Terms of Use: http://spiedl.org/terms

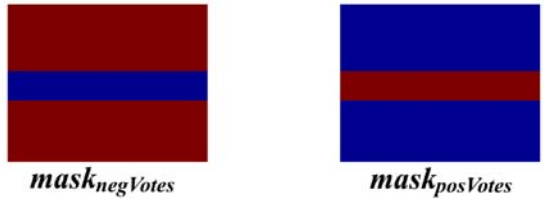

Figure 3. Images representing the two masks used to calculate *pVotes*. The red color stands for $true$, the blue for $false$.

the difference on each the coefficients

$$dR(x,y) = R(x,y+1) - R(x,y) \qquad \text{for} \quad 0 \leq y < \phi - 1 \tag{1}$$

where R is the normalised Radon transform having on the horizontal axis the different angles of projections and on the vertical one the number of projections for each angle. ϕ is the number of projections. The maxima locations of dR are calculated and stored in a new binary image dR_{max}. Two additional binary images are generated $mask_{posVotes}$ and $mask_{negVotes}$. The former contains ones only on a horizontal stripe at the center of the image and it represents the ideal path of the cliff; the height of the stripe depends on the size of the window and the parameters of the Radon transform, in our experiments we have employed a value of 3. $mask_{negVotes}$ is the complement image of $mask_{posVotes}$ as shown in Fig 3. A connected component analysis is run on dR_{max}, and the connected component which contains the highest value and passes through $mask_{posVotes}$ is labeled as $pathCand$. $pathCand$ contains the path that is more likely to represent the Gaussian object located at the center of the window, for this reason $pathCand$ will receive a positive vote for each of its pixel that overlays $mask_{posVotes}$ and a negative one for each pixel of the path corresponding to a positive value on $mask_{negVotes}$; see Fig 4 for some examples.

The *cumulative peak probability* (*CPP*) estimates a posterior probability of having a prominent peak with a constant height. For each ray in the Radon transform the following equations are used.

$$R_\mu(c) = \frac{1}{\phi}\sum_{n=1}^{\phi} R(n,c) \qquad \text{for} \quad 0 \leq c < \rho \tag{2}$$

$$R_\sigma(c) = \sqrt{\frac{1}{\phi - 1}\sum_{n=1}^{\phi}[R(n,c) - R_\mu(c)]^2} \qquad \text{for} \quad 0 \leq c < \rho \tag{3}$$

$$R_{\mu/\sigma} = \frac{R_\mu}{R_\sigma} \tag{4}$$

$$CPP = \frac{max(R_{\mu/\sigma}) - max_2(R_{\mu/\sigma})}{max(R_{\mu/\sigma})} \tag{5}$$

Where ρ is the length of each projection, $max(f)$ is the value of the maximum peak of f and $max_2(f)$ is the value of the second highest maximum peak of f.

2.2 Preprocessing / Candidate Selection

The background appearance of the human retina has significant variability from person to person and between racial groups. Additionally, the illumination changes pose an additional obstacle to the detection of microaneurysms on unprocessed images produced by fundus cameras. Our first approach to preprocessing was inspired by the method of Quellec et al. [4] A discrete stationary wavelet analysis is performed on the green channel of the image using the Haar basis up to the second scale. The illumination changes are for the most part located on the first scale because of their low frequency. If the image is reconstructed replacing the original first scale plane with zeros, the result obtained is a signed image [†] with the background removed. The image is further preprocessed by extracting only the negative pixels, inverting their value and

[†] In a signed image each pixel can have also a negative value.

Downloaded from SPIE Digital Library on 03 May 2010 to 128.219.49.8. Terms of Use: http://spiedl.org/terms

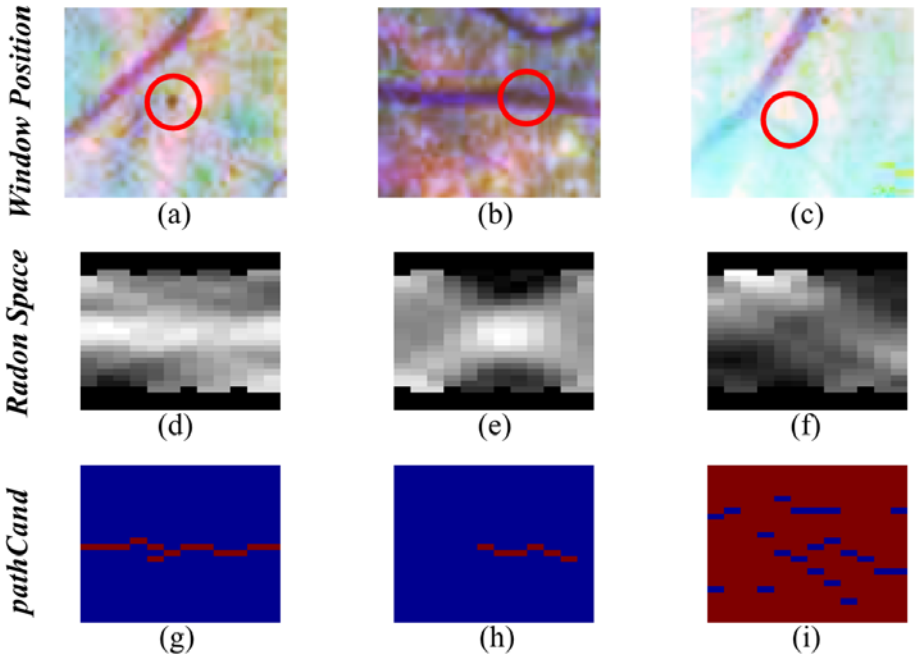

Figure 4. Examples of the *pathCand* output for various windows. In the first row we show the location of the circular window with a color-enhanced fundus image for illustration; in the second row the 2D view of the Radon transform in the window above; in the third row the *pathCand* found (shown in red). The *pVotes* obtained are: 13, 6 and -185 for (g) (h) and (i) respectively.

normalizing them from 0 to 255. This operation has the effect of discarding the peaks bright lesions, optic nerve, glare artifacts and some nerve fiber layer reflectance, while at the same time enhancing microaneurysms and vessels.

While this approach seemed to work particularly well on good quality images acquired with the Zeiss Visucam PRO fundus camera, for images of lower quality acquired with other fundus cameras this was not the case. This problem was particularly apparent on the dataset of the Retina On-line Challenge.[5] The reason is likely to be related with the low dynamic range and increased noise which negatively affected our Wavelet preprocessing that requires enough signal to be able to use only the negative pixels, and yet have a good enough representation of the image.

Our solution exploits the inherent strength of the Radon Cliff to background variations: we will employ it directly on the original image without any explicit image normalization. Instead, an initial rough candidate selection based on the color is performed to speed up further processing. The color image is normalized with the technique indicated by Cree et al.,[6] then the image is converted to grayscale[‡] and all the pixels having a value greater than $\varepsilon = 215$ are considered as potential candidates.

2.3 Microaneurysms Detection with Radon Cliff Operator

In the current experiment all the images are resized to a height of $750px$ maintaining the width/height ratio in order to simplify the selection of the parameters. A round sliding window ($17x17$) is centered on each candidate pixel px_{cand} and the Radon Cliff measures (*pVotes* and *CPP*) are obtained.

If $pVotes > 4$ the candidate is considered for further processing and the probability of being a microaneurysm P_{ma} is calculated as follows.

$$P_{col} = \frac{mean(normBlob(Px_{cand}) - \varepsilon)}{255 - \varepsilon} \tag{6}$$

$$P_{ma} = P_{col} \cdot CPPpx_{cand} \tag{7}$$

[‡]To convert the image to grayscale the weighted sum of the R, G and B component is employed: $V = 0.2989R + 0.5870G + 0.1140B$

Downloaded from SPIE Digital Library on 03 May 2010 to 128.219.49.8. Terms of Use: http://spiedl.org/terms

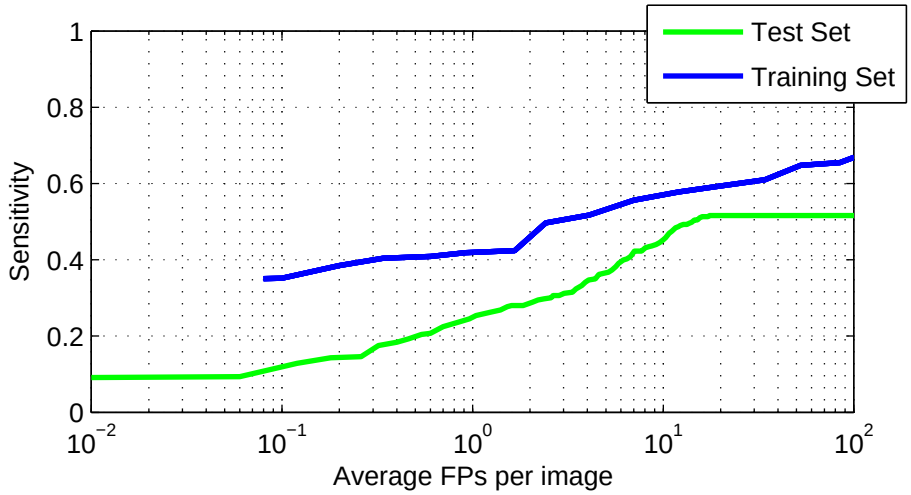

Figure 5. Algorithm performance on the ROC test and training set.

where $normBlob(Px_{cand})$ is the list of pixels contained in the connected blob extracted in the candidate selection phase; $mean(f)$ is the mean of f and $CPPpx_{cand}$ is the CPP measured on px_{cand}.

Some test images showed small dark spots at the edges of the Optic Nerve Cup and these structures can lead to false positives. In the literature there are various efficient methods to detect the location of the Optic Nerve (ON). Therefore, it is sufficient to find the center of the ON with one of them and remove all the microaneurysms detected too close to the ON. We have employed the hybrid technique developed by Karnowski et al. [7] to find the ON center and a fixed threshold of $\frac{1}{8}imageWidth$.

3. RESULTS

The algorithm was initially developed on anonymized images from a telemedicine study in Memphis, Tennessee, [8] then the publicly available dataset of the Retinopathy Online Challenge (ROC)[5] is used for testing purposes. The ROC dataset is composed of 100 color images divided in training and testing set; the images were all taken with Topcon NW 100, NW 200 or Canon CR5-45NM non-mydriatic cameras with a resolution ranging between 768x576 and 1394x1391 at the default JPEG compression settings. The ground truth is publicly available for the training set only.

Other authors[9,10] who have tested microaneurysm detection algorithms on the ROC dataset have noticed some problems with the ground truth publicly available; in some areas lesions are undistinguishable from the background. For this reason, we have removed all the lesions that were not visible with the naked eye from the ground truth of ROC training set. Then, we tested our algorithm on the amended training set and on the official testing set [§]. We are able to employ both sets, because our algorithm does not explicitly require any training phase. Fig 5 shows the functional ROC curve of the performance of the algorithm proposed on the two sets. The time required to analyze an image was ∼5 seconds with an unoptimized Matlab implementation running on a 2.27 GHz Intel Core 2 Duo machine.

4. DISCUSSION

The technique proposed is largely based on the two outputs of the Radon Cliff in order to show the discriminative ability of the features created with this operator. In our tests it was possible to achieve a sensitivity of 41% and 25% with a single false positive on average for each image. Considering that for screening purposes it is not always useful to identify all microaneurysms in each retina, the current output could be employed in this current form as a input of a screening system for diabetic retinopathy similar to the ones presented by Niemeijer et al. [11] or Chaum et al.[8]

[§]The ground truth for the testing set is not publicly available. We sent the segmented microaneurysm to the group responsible for the ROC and we have received the results back.

Downloaded from SPIE Digital Library on 03 May 2010 to 128.219.49.8. Terms of Use: http://spiedl.org/terms

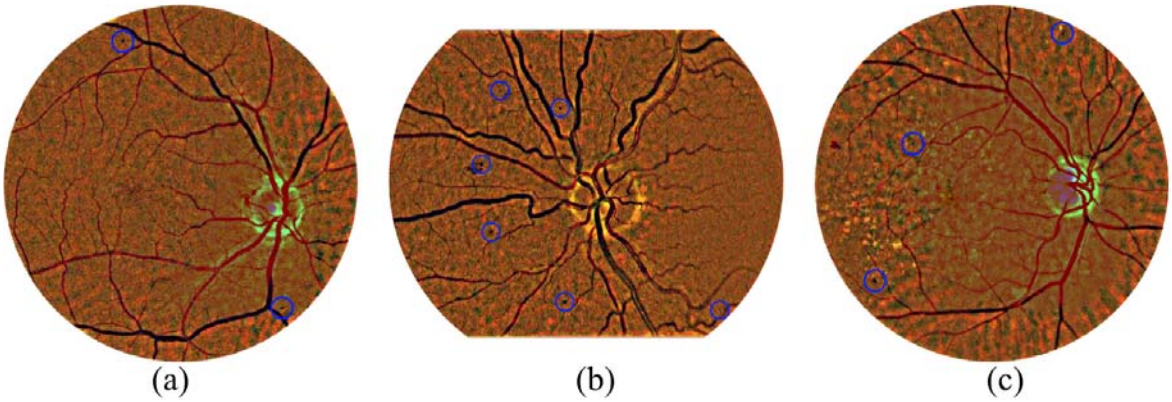

Figure 6. Examples of the microaneurysms segmentation with $P_{ma} > 0.1$. Note that the images shown are enhanced with the method of Cree et al.[6] in order to allow a better visibility of the lesions, but the Radon Cliff operator is applied on the original image.

Although the current results in the ROC dataset do not surpass all the other techniques found in the literature,[5] the Radon Cliff operator has various other advantages.

- No explicit training is required with standard pattern recognition techniques.
- Microaneurysms of different sizes can be identified without multiscale analysis.
- It works directly on the original image. Hence, any preprocessing step that might increase the noise in the image is avoided.
- It automatically distinguishes between vessels and microaneurysms.
- It can recognise microaneurysm close to the vasculature.

In some instances, the Radon Cliff's ability to recognize Gaussian structures close to the vessels is counterproductive. There are images that have darker round points on the vessels themselves which sometimes the Radon Cliff operator considers to be microaneurysm. A similar problem happens when small capillaries appear disconnected from the main vasculature; they generally look as very small skewed Gaussians and might be easily confused for microaneurysms. In the current implementation this is not of a great concern because they generally have a low probability score. Fig 6 shows some examples of the segmentation obtained.

5. CONCLUSION

In this study we have introduced a new way to pre-process a retinal fundus image which lays its ground on a novel operator based on the Radon transform which appears to be conceptually simple and very powerful. Its applications are not limited to lesion detection, but it could be employed successfully to any field of image processing where Gaussian shapes are normally detected with correlation filters.

The computational performance of the algorithm seems to be satisfactory, especially considering that the current implementation is created in an interpreted language as Matlab. In fact, there are vast margins of improvements with a native code implementation that exploits the parallelism exposed by modern CPUs or GPUs. The Radon Cliff operator is particularly suited to this because it performs a small set of relatively simple operations on many pixels and the output of the pixels are completely independent from each others.

In the near future we will employ the output of the Radon Cliff operator in conjunction with other detector of other types of lesions in order to evaluate the possibility of a reliable automatic system for screening diabetic retinopathy and other retina diseases.

Downloaded from SPIE Digital Library on 03 May 2010 to 128.219.49.8. Terms of Use: http://spiedl.org/terms

6. ACKNOWLEDGEMENTS

These studies were supported in part by grants from Oak Ridge National Laboratory, the National Eye Institute, (EY017065), by an unrestricted University of Tennessee Health Science Center Departmental grant from Research to Prevent Blindness, New York, NY, and by The Plough Foundation, Memphis, TN.

REFERENCES

[1] Resnick, J., "The radon transforms and some of its applications," *IEEE Transactions on Acoustics, Speech, and Signal Processing* **33**(1), 338–339 (1985).

[2] Kingston, A. and Autrusseau, F., "Lossless image compression via predictive coding of discrete radon projections," *Signal Processing: Image Communication* (2008).

[3] Liu, G., Lin, Z., and Yu, Y., "Radon representation-based feature descriptor for texture classification," *IEEE Trans on Image Proc* **18**, 921–928 (2009).

[4] Quellec, G., Lamard, M., Josselin, P. M., Cazuguel, G., Cochener, B., and Roux, C., "Optimal wavelet transform for the detection of microaneurysms in retina photographs," *IEEE Trans on Medical Imaging* **27**(9), 1230–1241 (2008).

[5] Niemeijer, M., van Ginneken, B., Cree, M. J., Mizutani, A., Quellec, G., Sanchez, C. I., Zhang, B., Hornero, R., Lamard, M., Muramatsu, C., Wu, X., Cazuguel, G., You, J., Mayo, A., Li, Q., Hatanaka, Y., Cochener, B., Roux, C., Karray, F., Garcia, M., Fujita, H., and Abramoff, M. D., "Retinopathy online challenge: Automatic detection of microaneurysms in digital color fundus photographs," *IEEE Transactions on Medical Imaging* **29**, 185–195 (Jan. 2010).

[6] Cree, M. J., Gamble, E., and Cornforth, D., "Colour normalisation to reduce interpatient and intra-patient variability in microaneurysm detection in colour retinal images," in [*WDIC2005 ARPS Workshop on Digital Image Computing*], (2005).

[7] Karnowski, T. P., Govindasamy, V. P., Tobin, K. W., and Chaum, E., "Locating the optic nerve in retinal images: comparing model-based and bayesian decision methods.," *Conf Proc IEEE Eng Med Biol Soc* **1**, 4436–4439 (2006).

[8] Chaum, E., Karnowski, T. P., Govindasamy, V. P., Abdelrahman, M., and Tobin, K. W., "Automated diagnosis of retinopathy by content-based image retrieval.," *Retina* **28**(10), 1463–1477 (2008).

[9] Zhang, B., Wub, X., Youc, J., Lic, Q., and Karray, F., "Hierarchical detection of red lesions in retinal images by multiscale correlation filtering," *Conf Proc of SPIE* **7260** (2009).

[10] Mizutani, A., Muramatsua, C., Hatanakab, Y., Suemoria, S., Haraa, T., and Fujitaa, H., "Automated microaneurysm detection method based on double-ring filter in retinal fundus images," *Conf Proc of SPIE* **7260** (2009).

[11] Niemeijer, M., Abramoff, M. D., and van Ginneken, B., "Information fusion for diabetic retinopathy cad in digital color fundus photographs," *IEEE Transactions on Medical Imaging* **28**(5), 775–785 (2009).

Downloaded from SPIE Digital Library on 03 May 2010 to 128.219.49.8. Terms of Use: http://spiedl.org/terms